Scanning tunneling microscopy studies of the cuprate superconductor $HgBa_2Ca_2Cu_3O_{8+\delta}$

Fan Zhang,[1,2,3] Xingyuan Hou,[1,2,4,5,*] Wenshan Hong,[6] Yubing Tu,[1,4,5] Tao Han,[1,4,5] Zongyuan Zhang,[1,4,5] Yuan Li,[6] and Lei Shan[1,2,4,5,7,†]

[1]*Information Materials and Intelligent Sensing Laboratory of Anhui Province, Institutes of Physical Science and Information Technology, Anhui University, Hefei 230601, China*

[2]*Center of High Magnetic Fields and Free Electron Lasers, Anhui University, Hefei 230601, China*

[3]*Beijing National Laboratory for Condensed Matter Physics, Institute of Physics, Chinese Academy of Sciences, Beijing 100190, China*

[4]*Leibniz International Joint Research Center of Materials Sciences of Anhui Province, Anhui University, Hefei 230601, China*

[5]*Key Laboratory of Structure and Functional Regulation of Hybrid Materials (Anhui University), Ministry of Education, Hefei 230601, China*

[6]*International Center for Quantum Materials, School of Physics, Peking University, Beijing 100871, China*

[7]*Hefei National Laboratory, Hefei 230088, China*

(Received 1 November 2023; revised 8 January 2024; accepted 26 January 2024; published 23 February 2024)

We report on scanning tunneling microscopy and spectroscopy studies of the slightly underdoped cuprate superconductor $HgBa_2Ca_2Cu_3O_{8+\delta}$, which has an onset $T_c \approx 120$ K. Disordered HgO-terminated surfaces were observed after sample cleaving in ultrahigh vacuum, revealing spatially inhomogeneous energy gaps with a low-lying V-shaped structure and the ubiquitous mode features. Similar to Bi-family cuprate superconductors, vortex cores were identified by the suppression of superconducting coherence peaks and the emergence of in-gap features. Superconductivity near step edges is also strongly suppressed over several coherence lengths, forming an effective interface to the superconducting region, where the local spectra show a weak zero-bias conductance peak arising from the Andreev bound states. These results are expected from the widely believed d-wave nature in cuprates, demonstrating a platform for studying unconventional superconductivity.

DOI: 10.1103/PhysRevB.109.085132

I. INTRODUCTION

Cuprate superconductors have attracted significant attention in condensed-matter physics for the high transition temperatures T_c above the liquid nitrogen temperature and potential applications. Despite detailed crystal structures, they can be viewed as alternating stacks of metal-oxygen charge reservoir layers and CuO_2 layers, where unconventional superconductivity emerges among strongly correlated electrons after carrier doping [1–3]. The microscopic mechanism remains one of the most important puzzles, whose systematic understanding is essential and benefits from some advanced experimental techniques such as scanning tunneling microscopy and spectroscopy (STM and STS). It plays a unique role in detecting the surface local density of states (LDOS) of electronic systems with high spatial and energy resolution and even extends to momentum space depending on the subsequently developed Fourier transform STM techniques [4–6]. The entangled unconventional superconductivity with coexisting symmetry-breaking orders has been well elaborated primarily focusing on the canonical hole-doped $Bi_2Sr_2Ca_{n-1}Cu_nO_{2n+4+\delta}$ (BSCCO) including B2212, B2201, and B2223, the ideal platforms that can be easily cleaved to expose excellent BiO planes for surface-sensitive experiments [7–11].

However, there is still doubt about whether the intrinsic information of the superconductivity can be detected because of the general difficulty in directly tunneling to the inner CuO_2 layer. In previous attempts, the exposed inner layers of BSCCO show quite distinct characteristics from the BiO layer, raising an issue of the layer-dependent spectroscopic properties of BSCCO [12]. Whereas it is beneficial to examine the consistency of tunneling spectra associated with superconductivity in other cuprates with similar crystalline structures but distinct carrier reservoir layers. However, the lack of material variations in STM and STS research on cuprates has been a long-standing issue. $Ca_xNa_{2-x}CuO_2Cl_2$ (Na-CCOC) is another van der Waals cuprate that can be easily cleaved. Nevertheless, Na-CCOC has a bit different structure with apical Cl atoms instead of O in the CuO_5 pyramids. Most importantly, its T_c is much lower than that of BSCCO [13], and always shows no well-defined coherence peaks in the tunneling spectra [14,15]. People also tend to alternative cuprates with higher T_c such as $YBa_2Cu_3O_{7-\delta}$ (YBCO) for STM and STS studies, although the additional CuO-chain layers result in some different results to BSCCO [16].

In some respects, $HgBa_2Ca_2Cu_3O_{8+\delta}$ (Hg1223) may be the most appropriate hole-doped cuprate for the comparison to the high-T_c BSCCO. On one hand, it possesses a crystal structure dramatically similar to BSCCO with apical O atoms in the CuO_5 pyramids and the absence of CuO-chain layers. On the other hand, Hg1223 has attracted considerable attention for the highest T_c value at ambient pressure, which is helpful to reveal more details of superconductivity [17].

*xyhou@ahu.edu.cn
†lshan@ahu.edu.cn

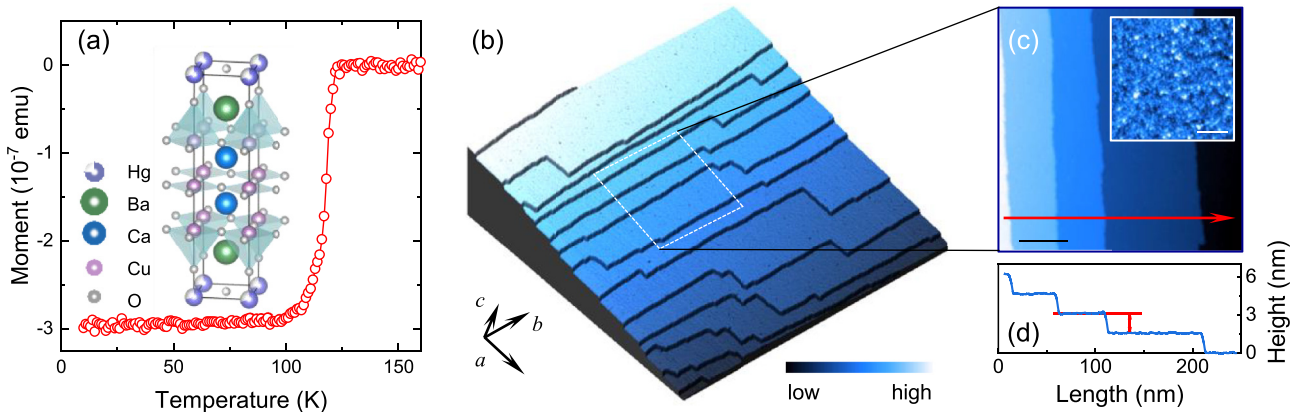

FIG. 1. (a) Temperature-dependent magnetic susceptibility of Hg1223 sample, which exhibit an onset T_c of ≈120 K. Inset shows the crystal structure of Hg1223 with inequivalent CuO_2 planes. (b) Topographic image with tunneling current $I_{set} = 4$ pA and bias voltage $V_b = -980$ mV. (c) Enlarged image of the surface shown in the dashed box in panel (b), the black scale bar represents 50 nm. The inset is a detailed image with high resolution taken from this area, and the white scale bar represents 10 nm. (d) The height of the profile along the arrow line in panel (c) indicates that the difference in step heights is equal to the height of one unit cell.

However, relevant results were rather rare to date for various difficulties in spectroscopic experiments on Hg1223 [18,19]. Benefiting from the recent breakthrough in single crystal growth [20], we attempt to perform STM and STS measurements on this system, which has different crystallographic structures and chemical composition in the charge reservoir layers to facilitate a deeper understanding of existing results on hole-doped cuprates.

In this paper, we have studied the superconducting properties of the slightly underdoped Hg-1223 single crystal on the disordered HgO layer by STM and STS. We obtained quite similar results about the low-energy electronic states, vortex states, the significant suppression of superconductivity, and the emergence of Andreev reflection near the edges. All the observations are consistent with the d-wave pairing symmetry in CuO_2 layers, meeting the expected extension of the planar wave function via the apical atoms. These results help facilitate a deeper understanding of this system and strengthen the deduced important issues of superconductivity in cuprates.

II. EXPERIMENT

The as-grown Hg1223 samples were synthesized by the high-pressure growth method with a primary T_c of about 105 K, then tuned by postannealing in air or oxygen atmosphere under different temperature conditions [20]. The studied sample in this work is slightly underdoped, whose onset T_c is about 120 K revealed from the magnetization measurements shown in Fig. 1(a). Commercial polycrystalline PtIr tips were used in the STM and STS measurements after being cleaned by e-beam heating and calibrated on the Au(111) surface. The samples were mechanically cleaved in an ultrahigh vacuum (UHV) environment at the liquid nitrogen temperature to expose a fresh surface. The STM topography was acquired in the constant-current mode with bias voltage V_b applied to the sample, and the differential conductance (dI/dV) spectra were measured by using a standard lock-in technique with a modulation frequency of 973.1 Hz. All the presented data were obtained at 4.8 K.

III. RESULTS AND DISCUSSION

As illustrated by the schematic crystal structure in the inset of Fig. 1(a), Hg1223 has a layered structure with the space group of $P4/mmm$ and tetragonal lattice constants $a = b = 3.85$ Å and $c = 15.86$ Å [17,20]. It comprises two distinct types of inequivalent CuO_2 planes resembling the familiar trilayer cuprate B2223, in which one pure inner CuO_2 plane (IP) is sandwiched between two outer CuO_2 planes (OPs) in the edge-sharing CuO_5 pyramids with the apical O [21,22]. The carrier reservoir blocks are acted by the HgO, BaO, and Ca layers lying between the nonequivalent superconducting CuO_2 planes. Different from BSCCO and Na-CCOC, a natural cleavage plane along the c axis is absent because the HgO layer is shared by two adjacent unit cells. Therefore, the cleavage of the sample needs to break at the weakest chemical bonding along the c axis in STM experiments, which could not occur within the CuO_2 layers because of their strong chemical bonds [12,23]. Figure 1(b) displays an 800 nm × 800 nm topographic image of the cleaved Hg1223 sample. In the field of view, the exposed surface shows numerous terraces with varied widths ranging from dozens of nanometers to more than one hundred nanometers. Corresponding to the expectation in a tetragonal lattice, the step edges are either roughly parallel or perpendicular to each other, although subtle deviation could be noticed in the enlarged image in Fig. 1(c). However, a completely disordered surface with clusters spreading all over is always observed in the atomic view displayed in the inset of Fig. 1(c), preventing us from identifying the cleaved planes from atomic lattice. We attempt to distinguish them from the topographic height distribution [12]. A striking observation is that all the steps have nearly the same height, which can be seen in a profile in Fig. 1(d) along the red arrow in Fig. 1(c). The step height is estimated to be 1.6 nm, equal to the height of one unit cell. This suggests that the exposed surfaces should only be the HgO terminal layers because of the nonunique spaces between the other layers.

Similar cleavage usually occurs in materials without natural cleaved planes, leaving approximately half mounts of

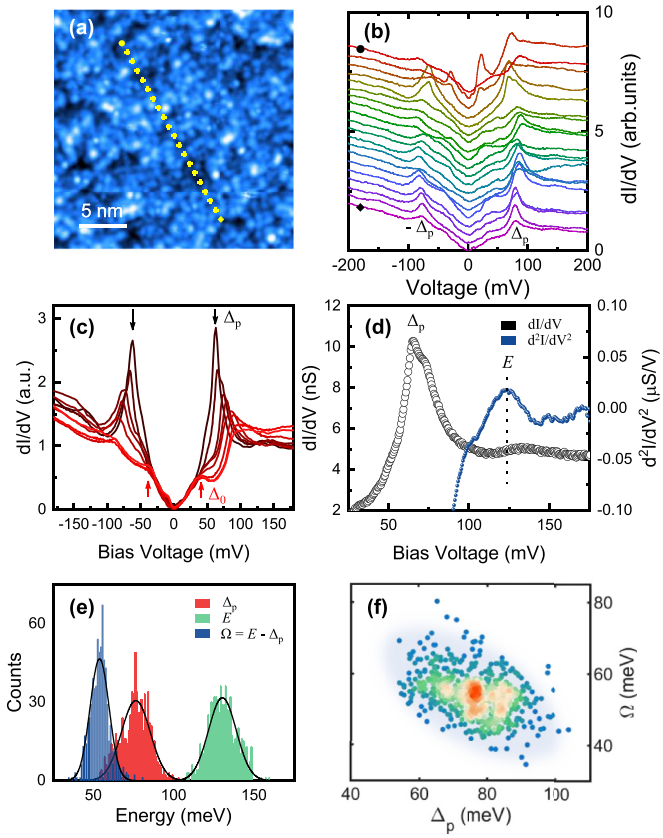

FIG. 2. (a) A zoom-in image taken with the condition $V_b = -1$ V and $I = 3$ pA. (b) Spatially resolved dI/dV spectra along the trajectory in panel (a). Spectra are offset for clarity. The diamond and circle symbols represent the starting and ending points, respectively. (c) Some typical dI/dV spectra sorted by Δ_p. (d) A representative dI/dV spectrum and its derivative d^2I/dV^2 curve. The peak in derivative d^2I/dV^2 is labeled E, corresponding to the dip-hump structures in dI/dV spectrum. (e) Statistical histograms of the energy gap Δ_p, the EBC energy E, and the corresponding mode energy Ω. (f) Statistical anticorrelation between Δ_p and Ω.

atoms on the exposed surface to maintain charge neutrality [24–28]. The disordered Hg and O atoms bring about dramatically distinct conditions from BSCCO or Na-CCOC, as displayed in Fig. 2(a), while the measured tunneling spectra are highly similar to the previously reported STM and STS results in BSCCO. In Fig. 2(b), we show the measured spatially resolved spectra at the locations marked by the crosses in Fig. 2(a). Most tunneling spectra exhibit prominent coherence peaks with varied Δ_p accompanied by robust low-lying in-gap kinks and a V-shaped structure near Fermi energy, indicating the presence of nodes in superconducting order parameters [4–6]. Some spectra are occasionally observed as complex in-gap features accompanied by a distinct background attribute to the unrecognized disorders or defects. However, it is difficult to identify them in this situation. The coexistence of two energy scales is similar to other underdoped cuprates [4–6]. To clarify this issue better, Fig. 2(c) shows some typical dI/dV spectra sorted by the local gap size. The sharp coherence peaks become broad with the increasing energy gap, while the kinks at the energy of Δ_0 keep homogenous despite the inhomogeneous Δ_p. These low-lying kinks were regarded as the signature of the superconducting gap opened near the nodal region in previous measurements on BSCCO, where the quasiparticle states are revealed to be quite coherent against local carrier density [4,5,29,30]. However, the quasiparticles in the antinodal region corresponding to the pseudogaps are substantially sensitive to local doping levels, leading to the spatial variation of Δ_p in underdoped samples [4,5]. Noticeably, there is a small kink on the shoulder of the coherence peak in some dI/dV spectra. As reported before, the different hole concentrations in OPs and IP result in a prevalent two-gap feature in optimally doped to over doped B2223 [21,22,31–33]. Presumably, this small kink is also related to multiple CuO_2 layers in this system, which needs more accurate inspections.

Another important observation is the fingerprint of the ubiquitous electron-boson couplings (EBCs), which is crucial for understanding the still unclear pairing mechanisms [34–38]. As shown more clearly in Fig. 2(d), there is at least one broad dip-hump structure at the symmetric energy E outside the main coherence peaks. This feature could also be characterized by a peak (or a dip in negative voltage) in the second derivative d^2I/dV^2 [25,39–47]. Then the corresponding mode energy Ω is deduced by subtracting Δ_p from E. On account of the spatially electronic inhomogeneity at the nanoscale, the associated local properties vary substantially all over the sample surface. Figure 2(e) displays the statistical histograms of Δ_p, E, and the corresponding Ω extracted from a large number of tunneling spectra. Their normal distributions are fitted with the mean values of about 76, 130, and 54 meV, respectively. The presence of the EBC features in Hg1223 suggests that they might have the same origin as other cuprates, mainly concerned as phonon, magnetic excitation, or together [34–38]. They are manifested as antinodal 40–50 meV and nodal 70–80 meV quasiparticle dispersion kinks in other cuprates [34–37,48]. Our obtained mode energy of Hg1223 is close to the 50 meV dispersion kink along the antinodal direction, which is still unclear on its relation to the oxygen buckling mode or magnetic resonance mode [49–55]. The isotope effect of this mode in B2212 favors the lattice vibrations as its origin [40,56]. While the ratio Ω/k_BT_c is estimated to be about 5.2, also close to the spin-resonance mode in neutron scattering with a ratio of 5–6 [37,57–59]. Thus, the interpretation of the EBCs in Hg1223 remains controversial for the similar energy scale. For better qualitative analysis, we present the dependence of the bosonic mode Ω on the energy gap Δ_p in Fig. 2(f). The mode energies show anticorrelation with the gaps similar to the case in BSCCO, phenomenologically suggesting an intimate interplay between collective modes and superconductivity [36,39–44]. The further understanding in this system is crucial for exploring the still unknown pairing mechanism in high-T_c superconductors together with the interpretation of other experimental results, such as optical experiments, ARPES, and inelastic neutron scattering.

When a magnetic field is applied perpendicularly to the Hg1223 sample surface, the modified electronic states in vortex cores make it possible to image them by zero-bias conductance (ZBC) mapping. Figure 3(a) shows the ZBC map measured at 0 T, demonstrating that the sample exhibits

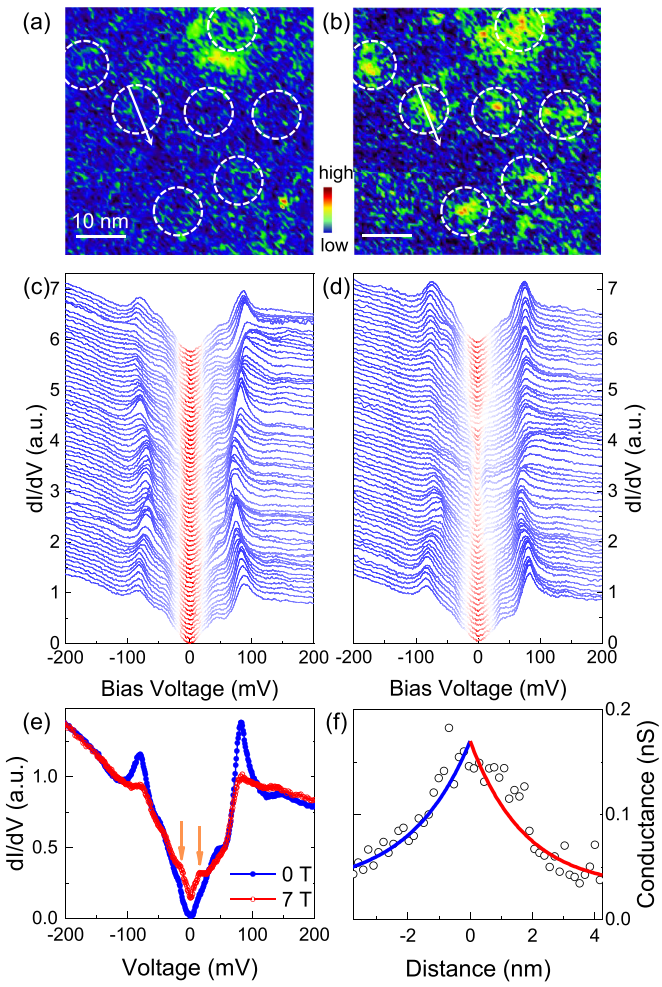

FIG. 3. (a), (b) ZBC map measured at 0 and 7 T in the same FOV, the white scale bar represents 10 nm. The ZBC at 0 T shows the widespread superconductivity accompanied by localized impurity resonances, while ZBC at 7 T reveals vortices distribution for the local conductance enhancement. The experimental conditions are $V_b = -250$ mV, $I = 0.25$ nA, and $V_m = 2$ mV. (c), (d) Spatially resolved dI/dV spectra at 0 and 7 T, taken along the same trajectory indicated by the white arrows in panels (a) and (b) across a vortex center. The experimental conditions are $V_b = -250$ mV, $I = 0.25$ nA, and $V_m = 2$ mV. (e) Comparative analysis of tunneling spectra between the vortex center at 7 T and the identical position at 0 T. The orange arrows denote the in-gap vortex bound states. (f) ZBC evolution extracted from the spectra across the vortex, approximately following a simple-exponential decay tendency.

ubiquitous superconductivity in large areas except for some anomalous defect states as mentioned above. After applying a magnetic field of 7 T in the same field of view (FOV), we found that ZBC in some regions (in white dashed circles) is additionally enhanced owing to the formation of the vortex bound states. The vortices are not rearranged into an ordered lattice but tend to reside in the regions containing aggregate defects, as a result of the strong defect pinning effect [60]. To avoid the influence of the defect resonance states, the study of vortex states should be performed in regions without defects. We thus compared the tunneling spectra at 0 and 7 T along the same trajectory denoted by the white arrows in Figs. 3(a) and 3(b), respectively. As displayed in Fig. 3(c), the tunneling spectra measured at 0 T show uniform low-energy states near E_F, although the coherence peaks still manifest spatial electronic inhomogeneity [4–6]. In contrast, low-lying in-gap states emerge in the vortex core, appearing as the visual shrinkage of the red color in Fig. 3(d). Figure 3(e) represents the spectra taken from the vortex core at 7 T and the same location at 0 T, with an overlapped background in large voltage. The spectrum at the vortex core center shows strong suppression of the coherence peaks at the superconducting gap edge, and the appearance of a pair of in-gap peaks with energies near 15 meV, as indicated by the orange arrows. Similar to the vortex bound states in BSCCO, the density of states at E_F is elevated from zero without the formation of a zero-bias conductance peak observed in the conventional superconductors [61–63]. The vortex states are distinguishable as the spectral features within only a short distance. We trace the zero-bias conductance values from the evolution of the tunneling spectra and depicted them in Fig. 3(f). The characteristic recovery distance of superconductivity is deduced to be about 1.8 nm from the exponential decay of the zero-bias conductance, producing an estimation of the short superconducting coherence length ξ_{ab}.

Therefore, an expected suppression of superconductivity should be observed in the vicinity of the step edges, where the spatial continuity of the superconducting order parameters is significantly broken [64]. We then examined the DOS of a large terrace terminated by a rectangular corner as depicted in Fig. 4(a). The anomalous electronic states near the edges are highlighted by the ZBC enhancement as shown in Fig. 4(b). The extending length of the edge states is estimated to be 2–4 nm from the DOS image. As shown in Fig. 4(c), the point spectra taken near the edges indeed reveal a significant suppression of the coherence peaks and filling in of the superconducting gap. Another striking feature on some spectra is observed as a remarkable ZBC peak in addition to the suppression of superconductivity. It is quite different from resonance states induced by defects and is absent in the region far from step edges in Fig. 4(b). These phenomena occurring at this effective normal metal–superconductor interference are reminiscent of the Andreev bound states (ABSs) in cuprate superconductors, expected as a degenerate accumulation of electronic states at E_F when the quasiparticle trajectories undergo a π phase change of superconducting order parameter [65–68].

In d-wave superconductors, the order parameter has a sign reversal across the nodal direction or, equivalently at an angle of $\pi/4$ with respect to the Cu–O bond in CuO_2 plane [34,35]. Therefore, no ABS is expected for step edges strictly parallel to the Cu–O bond because of the phase conservation for any specular reflection trajectories. However, for arbitrary orientation of the step edge relative to the Cu–O bond, sign reversal can also occur within a certain incidence angular range [65,68,69]. While the subtle deviation from the Cu–O bonds, evinced by the small angles between the step tendency, seems to explain the occurrence of the ABS, the nonsmoothed step edges may account for their point-like distribution. In principle, there will always be a sign reversal for some quasiparticle trajectories undergoing diffusive reflection around the

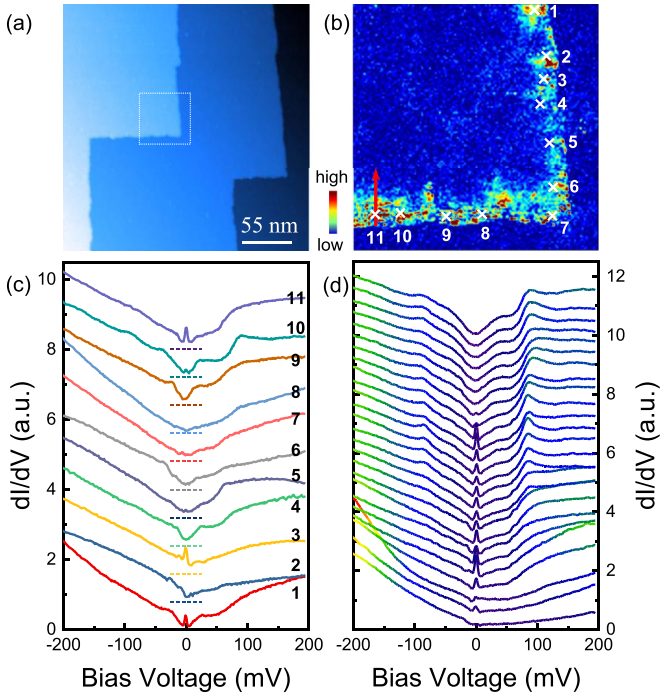

FIG. 4. (a) A topographic image of a 275 nm square field of view, showing the approximately perpendicular step edges ($V_b = -980$ mV and $I = 4$ pA). (b) ZBC map in the 60 nm × 60 nm area shown in the white dashed box of panel (a), exhibiting the suppression of superconductivity near the step edge. (c) Representative dI/dV spectra taken from random positions marked by the crosses in panel (b). Spectra are shifted vertically for clarity. (d) dI/dV spectra obtained along the trajectory shown by the arrow in panel (b). Spectra are shifted vertically for clarity. The experimental conditions in panels [(b)–(d)] are $V_b = -200$ mV, $I = 0.25$ nA, and $V_m = 2$ mV.

rough grains on step edges [65,68,69]. The ABS may also be completely smeared out by extensive diffusive reflection [67]. We then further investigated the evolution of ABS from the step edge by measuring tunneling spectra along the red arrow in Fig. 4(b) and presenting them in Fig. 4(d). It is found that superconductivity is significantly suppressed within a coherence length from the step edge. Once the spectrum weight of the coherence peaks begins to recover, a zero-bias peak associated with the ABS emerges and gradually builds up at the constructive interface. To be noticed, the ABS extends approximately 5 nm transverse to the step edge, which is longer than the recovery length of superconductivity.

The present STM and STS measurements on Hg1223 appear to show behaviors essentially identical to the BSCCO samples near the optimally doped range. As well as the consistency of the experimental data in slightly doped BSCCO and Na-CCOC, it may naturally lead to the phenomenological conclusion that STM and STS probes the electronic states of the common CuO_2 planes despite there are the significantly distinct barrier layers in these compounds. Most observations, in particular the ABS in the vicinity of step edges, meet the expectation of a d-wave pairing symmetry in this system. However, there is also a debate on the pairing symmetry of cuprates from phase sensitive techniques [70–72]. Therefore, an adequate theoretical mechanism for unconventional superconductivity should be able to simultaneously describe all the measured phenomena, which also needs more experiments on variable compounds to draw a definite conclusion. On one hand, phase sensitive quasiparticle interference measurements deserve to be carried out after overcoming the disordering problems. On the other hand, although any other atomic layers are not observed in this experiment, the mechanical cleavage of Hg1223 may also reserve the possibility to expose the other atomic layers for the lack of natural cleavage. It has the potential to clarify the roles played by the ingredient layers and shed light on the related controversies. These demonstrate the system as another reliable platform for STM to study high-T_c superconductivity and other relevant strongly correlated physics.

IV. CONCLUSION

In conclusion, we performed STM and STS experiments on the high-quality cuprate superconductor $HgBa_2Ca_2Cu_3O_{8+\delta}$ with an onset $T_c \approx 120$ K. The HgO-terminated surface is identified after cleavage, and the energy gaps on this surface are spatially inhomogeneous, with typical V-shaped characteristics. The vortex state can be determined by the significant suppression of the coherence peaks and the enhancement of the in-gap density of states, consistent with cuprates such as the BSCCO. At the step edge, the spectra have weak ZBCP characteristics originating from the Andreev-bound states. Taken together, these effects provide proof for d-wave superconductivity in Hg1223, and also render it a practical platform to investigate the intrinsic pairing mechanisms by state-of-the-art spectroscopic methods.

Note. Recently, Ref. [73] appeared, which reported large superconducting gap values in optimally-doped Hg1223. The statistical distribution of the observed gap values is consistent with our results.

ACKNOWLEDGMENTS

We are grateful to Prof. L. Zhao for fruitful discussions. This work was financially supported by the National Key R&D Program of China (Grant No. 2022YFA1403203), the Innovation Program for Quantum Science and Technology (Grant No. 2021ZD0302802), the National Natural Science Foundation of China (Grants No. 12074002 and No. 12374133), the Major Basic Program of Natural Science Foundation of Shandong Province (Grant No. ZR2021ZD01), and the Education Department of Anhui Province (Grant No. 2023AH020004). The crystal-growth work at Peking University was supported by the National Natural Science Foundation of China (Grants No. 12061131004 and No. 11888101). W.H. acknowledges support from the Postdoctoral Innovative Talent program (BX2021018) and the China Postdoctoral Science Foundation (2021M700250).

[1] E. Dagotto, Rev. Mod. Phys. **66**, 763 (1994).
[2] P. A. Lee, N. Nagaosa, and X.-G. Wen, Rev. Mod. Phys. **78**, 17 (2006).
[3] C. Proust and L. Taillefer, Annu. Rev. Condens. Matter Phys. **10**, 409 (2019).
[4] O. Fischer, M. Kugler, I. Maggio-Aprile, C. Berthod, and C. Renner, Rev. Mod. Phys. **79**, 353 (2007).
[5] K. Fujita, A. R.Schmidt, E.-A. Kim, M. J. Lawler, D. H. Lee, J. Davis, H. Eisaki, and S.-i. Uchida, J. Phys. Soc. Jpn. **81**, 011005 (2012).
[6] A. Yazdani, E. H. da Silva Neto, and P. Aynajian, Annu. Rev. Condens. Matter Phys. **7**, 11 (2016).
[7] A. N. Pasupathy, A. Pushp, K. K. Gomes, C. V. Parker, J. Wen, Z. Xu, G. Gu, S. Ono, Y. Ando, and A. Yazdani, Science **320**, 196 (2008).
[8] P. Cai, W. Ruan, Y. Peng, C. Ye, X. Li, Z. Hao, X. Zhou, D.-H. Lee, and Y. Wang, Nat. Phys. **12**, 1047 (2016).
[9] M. H. Hamidian, S. D. Edkins, S. H. Joo, A. Kostin, H. Eisaki, S. Uchida, M. J. Lawler, E.-A. Kim, A. P. Mackenzie, K. Fujita *et al.*, Nature (London) **532**, 343 (2016).
[10] S. Wan, H. Li, P. Choubey, Q. Gu, H. Li, H. Yang, I. M. Eremin, G. Gu, and H.-H. Wen, Proc. Natl. Acad. Sci. USA **118**, e2115317118 (2021).
[11] S. M. O'Mahony, W. Ren, W. Chen, Y. X. Chong, X. Liu, H. Eisaki, S. Uchida, M. H. Hamidian, and J. C. S. Davis, Proc. Natl. Acad. Sci. USA **119**, e2207449119 (2022).
[12] Y.-F. Lv, W.-L. Wang, J.-P. Peng, H. Ding, Y. Wang, L. Wang, K. He, S.-H. Ji, R. Zhong, J. Schneeloch *et al.*, Phys. Rev. Lett. **115**, 237002 (2015).
[13] Z. Hiroi, N. Kobayashi, and M. Takano, Nature (London) **371**, 139 (1994).
[14] T. Hanaguri, C. Lupien, Y. Kohsaka, D.-H. Lee, M. Azuma, M. Takano, H. Takagi, and J. C. Davis, Nature (London) **430**, 1001 (2004).
[15] T. Hanaguri, Y. Kohsaka, J. C. Davis, C. Lupien, I. Yamada, M. Azuma, M. Takano, K. Ohishi, M. Ono, and H. Takagi, Nat. Phys. **3**, 865 (2007).
[16] D. J. Derro, E. W. Hudson, K. M. Lang, S. H. Pan, J. C. Davis, J. T. Markert, and A. L. de Lozanne, Phys. Rev. Lett. **88**, 097002 (2002).
[17] A. Schilling, M. Cantoni, J. D. Guo, and H. R. Ott, Nature (London) **363**, 56 (1993).
[18] G. I. Meijer, C. Rossel, J. Karpinski, H. Schwer, R. Molinski, and K. Conder, Czech. J. Phys. B **46**, 1347 (1996).
[19] J. Y. T. Wei, C. C. Tsuei, P. J. M. van Bentum, Q. Xiong, C. W. Chu, and M. K. Wu, Phys. Rev. B **57**, 3650 (1998).
[20] L. Wang, X. Luo, J. Li, J. Zeng, M. Cheng, J. Freyermuth, Y. Tang, B. Yu, G. Yu, M. Greven *et al.*, Phys. Rev. Mater. **2**, 123401 (2018).
[21] Z. Hao, C. Zou, X. Luo, Y. Ji, M. Xu, S. Ye, X. Zhou, C. Lin, and Y. Wang, Phys. Rev. Lett. **125**, 237005 (2020).
[22] C. Zou, Z. Hao, H. Li, X. Li, S. Ye, L. Yu, C. Lin, and Y. Wang, Phys. Rev. Lett. **124**, 047003 (2020).
[23] Y. F. Lv, W. L. Wang, H. Ding, Y. Wang, Y. Ding, R. Zhong, J. Schneeloch, G. D. Gu, L. Wang, K. He, S. H. Ji, L. Zhao, X. J. Zhou, C. L. Song, X. C. Ma, and Q. K. Xue, Phys. Rev. B **93**, 140504(R) (2016).
[24] T. Kato, S. Okitsu, and H. Sakata, Phys. Rev. B **72**, 144518 (2005).
[25] Y. Fasano, I. Maggio-Aprile, N. D. Zhigadlo, S. Katrych, J. Karpinski, and O. Fischer, Phys. Rev. Lett. **105**, 167005 (2010).
[26] L. Shan, Y.-L. Wang, B. Shen, B. Zeng, Y. Huang, A. Li, D. Wang, H. Yang, C. Ren, Q.-H. Wang *et al.*, Nat. Phys. **7**, 325 (2011).
[27] J.-X. Yin, X.-X. Wu, J. Li, Z. Wu, J.-H. Wang, C.-S. Ting, P.-H. Hor, X. J. Liang, C. L. Zhang, P. C. Dai *et al.*, Phys. Rev. B **102**, 054515 (2020).
[28] M. L. Teague, G. K. Drayna, G. P. Lockhart, P. Cheng, B. Shen, H.-H. Wen, and N.-C. Yeh, Phys. Rev. Lett. **106**, 087004 (2011).
[29] K. McElroy, D.-H. Lee, J. E. Hoffman, K. M. Lang, J. Lee, E. W. Hudson, H. Eisaki, S. Uchida, and J. C. Davis, Phys. Rev. Lett. **94**, 197005 (2005).
[30] J.-H. Ma, Z.-H. Pan, F. C. Niestemski, M. Neupane, Y.-M. Xu, P. Richard, K. Nakayama, T. Sato, T. Takahashi, H.-Q. Luo *et al.*, Phys. Rev. Lett. **101**, 207002 (2008).
[31] S. Kunisada, S. Adachi, S. Sakai, N. Sasaki, M. Nakayama, S. Akebi, K. Kuroda, T. Sasagawa, T. Watanabe, S. Shin *et al.*, Phys. Rev. Lett. **119**, 217001 (2017).
[32] S. Ideta, K. Takashima, M. Hashimoto, T. Yoshida, A. Fujimori, H. Anzai, T. Fujita, Y. Nakashima, A. Ino, M. Arita *et al.*, Phys. Rev. Lett. **104**, 227001 (2010).
[33] X. Luo, H. Chen, Y. Li, Q. Gao, C. Yin, H. Yan, T. Miao, H. Luo, Y. Shu, Y. Chen *et al.*, Nat. Phys. **19**, 1841 (2023).
[34] A. Damascelli, Z. Hussain, and Z.-X. Shen, Rev. Mod. Phys. **75**, 473 (2003).
[35] J. A. Sobota, Y. He, and Z.-X. Shen, Rev. Mod. Phys. **93**, 025006 (2021).
[36] M. Eschrig, Adv. Phys. **55**, 47 (2006).
[37] G. Yu, Y. Li, E. M. Motoyama, and M. Greven, Nat. Phys. **5**, 873 (2009).
[38] Z. Li, M. Wu, Y.-H. Chan, and S. G. Louie, Phys. Rev. Lett. **126**, 146401 (2021).
[39] J. F. Zasadzinski, L. Ozyuzer, N. Miyakawa, K. E. Gray, D. G. Hinks, and C. Kendziora, Phys. Rev. Lett. **87**, 067005 (2001).
[40] J. Lee, K. Fujita, K. McElroy, J. A. Slezak, M. Wang, Y. Aiura, H. Bando, M. Ishikado, T. Masui, J.-X. Zhu *et al.*, Nature (London) **442**, 546 (2006).
[41] N. Jenkins, Y. Fasano, C. Berthod, I. Maggio-Aprile, A. Piriou, E. Giannini, B. W. Hoogenboom, C. Hess, T. Cren, and O. Fischer, Phys. Rev. Lett. **103**, 227001 (2009).
[42] F. C. Niestemski, S. Kunwar, S. Zhou, S. Li, H. Ding, Z. Wang, P. Dai, and V. Madhavan, Nature (London) **450**, 1058 (2007).
[43] P. Das, M. R. Koblischka, H. Rosner, T. Wolf, and U. Hartmann, Phys. Rev. B **78**, 214505 (2008).
[44] S. Pilgram, T. M. Rice, and M. Sigrist, Phys. Rev. Lett. **97**, 117003 (2006).
[45] L. Shan, J. Gong, Y.-L. Wang, B. Shen, X. Hou, C. Ren, C. Li, H. Yang, H.-H. Wen, S. Li *et al.*, Phys. Rev. Lett. **108**, 227002 (2012).
[46] S. Chi, S. Grothe, R. Liang, P. Dosanjh, W. N. Hardy, S. A. Burke, D. A. Bonn, and Y. Pennec, Phys. Rev. Lett. **109**, 087002 (2012).
[47] C.-L. Song, Y.-L. Wang, Y.-P. Jiang, Z. Li, L. Wang, K. He, X. Chen, J. E. Hoffman, X.-C. Ma, and Q.-K. Xue, Phys. Rev. Lett. **112**, 057002 (2014).
[48] H. Yan, J. M. Bok, J. He, W. Zhang, Q. Gao, X. Luo, Y. Cai, Y. Peng, J. Meng, C. Li *et al.*, Proc. Natl. Acad. Sci. USA **120**, e2219491120 (2023).

[49] L. J. P. Ament, M. van Veenendaal, T. P. Devereaux, J. P. Hill, and J. van den Brink, Rev. Mod. Phys. **83**, 705 (2011).
[50] T. P. Devereaux, T. Cuk, Z.-X. Shen, and N. Nagaosa, Phys. Rev. Lett. **93**, 117004 (2004).
[51] S. R. Park, D. J. Song, C. S. Leem, C. Kim, C. Kim, B. J. Kim, and H. Eisaki, Phys. Rev. Lett. **101**, 117006 (2008).
[52] C. Thomsen, M. Cardona, B. Gegenheimer, R. Liu, and A. Simon, Phys. Rev. B **37**, 9860 (1988).
[53] H. F. Fong, P. Bourges, Y. Sidis, L. P. Regnault, A. Ivanov, G. D. Gu, N. Koshizuka and B. Keimer, Nature (London) **398**, 588 (1999).
[54] M. K. Chan, C. J. Dorow, L. Mangin-Thro, Y. Tang, Y. Ge, M. J. Veit, G. Yu, X. Zhao, A. D. Christianson, J. T. Park, Y. Sidis, P. Steffens, D. L. Abernathy, P. Bourges, and M. Greven, Nat. Commun. **7**, 10819 (2016).
[55] Y. Li, V. Balédent, G. Yu, N. Barišić, K. Hradil, R. A. Mole, Y. Sidis, P. Steffens, X. Zhao, P. Bourges *et al.*, Nature (London) **468**, 283 (2010).
[56] G.-H. Gweon, T. Sasagawa, S. Y. Zhou, J. Graf, H. Takagi, D.-H. Lee, and A. Lanzara, Nature (London) **430**, 187 (2004).
[57] H. He, Y. Sidis, P. Bourges, G. D. Gu, A. Ivanov, N. Koshizuka, B. Liang, C. T. Lin, L. P. Regnault, E. Schoenherr *et al.*, Phys. Rev. Lett. **86**, 1610 (2001).
[58] H. He, P. Bourges, Y. Sidis, C. Ulrich, L. P. Regnault, S. Pailhès, N. S. Berzigiarova, N. N. Kolesnikov, and B. Keimer, Science **295**, 1045 (2002).
[59] J. Yang, J. Hwang, E. Schachinger, J. P. Carbotte, R. P. S. M. Lobo, D. Colson, A. Forget, and T. Timusk, Phys. Rev. Lett. **102**, 027003 (2009).
[60] H. Suderow, I. Guillamón, J. G. Rodrigo, and S. Vieira, Supercond. Sci. Technol. **27**, 063001 (2014).
[61] I. Maggio-Aprile, C. Renner, A. Erb, E. Walker, and O. Fischer, Phys. Rev. Lett. **75**, 2754 (1995).
[62] S. H. Pan, E. W. Hudson, A. K. Gupta, K.-W. Ng, H. Eisaki, S. Uchida, and J. C. Davis, Phys. Rev. Lett. **85**, 1536 (2000).
[63] T. Machida, Y. Kohsaka, K. Matsuoka, K. Iwaya, T. Hanaguri, and T. Tamegai, Nat. Commun. **7**, 11747 (2016).
[64] S. Misra, S. Oh, D. J. Hornbaker, T. DiLuccio, J. N. Eckstein, and A. Yazdani, Phys. Rev. Lett. **89**, 087002 (2002).
[65] T. Löfwander, V. S. Shumeiko, and G. Wendin, Supercond. Sci. Technol. **14**, R53 (2001).
[66] C.-R. Hu, Phys. Rev. Lett. **72**, 1526 (1994).
[67] S. Kashiwaya and Y. Tanaka, Rep. Prog. Phys. **63**, 1641 (2000).
[68] G. Deutscher, Rev. Mod. Phys. **77**, 109 (2005).
[69] Y. Tanaka and S. Kashiwaya, Phys. Rev. Lett. **74**, 3451 (1995).
[70] Q. Li, Y. N. Tsay, M. Suenaga, R. A. Klemm, G. D. Gu, and N. Koshizuka, Phys. Rev. Lett. **83**, 4160 (1999).
[71] Y. Zhu, M. Liao, Q. Zhang, H.-Y. Xie, F. Meng, Y. Liu, Z. Bai, S. Ji, J. Zhang, K. Jiang *et al.*, Phys. Rev. X **11**, 031011 (2021).
[72] H. Wang, Y. Zhu, Z. Bai, Z. Wang, S. Hu, H.-Y. Xie, X. Hu, J. Cui, M. Huang, J. Chen *et al.*, Nat. Commun. **14**, 5201 (2023).
[73] C. Wen, Z. Hou, A. Akbari, K. Chen, W. Hong, H. Yang, I. Eremin, Y. Li, H.-H. Wen, arXiv:2401.17079.